Reactions of Fe with H_2O and FeO with H_2. A Combined Matrix Isolation FTIR and Theoretical Study

Luning Zhang, Mingfei Zhou,* Limin Shao, Wenning Wang, Kangnian Fan, and Qizong Qin

Department of Chemistry, Laser Chemistry Institute, Fudan University, Shanghai 200433, People's Republic of China

Received: March 9, 2001; In Final Form: May 2, 2001

The study of the reactions of transition metal atoms with water is continued in this work. Here we report the study of the reactions of Fe with H_2O and FeO with H_2. In agreement with previous thermal atom experiments, laser-ablated Fe atoms reacted with H_2O to form the $FeOH_2$ and HFeOH molecules as characterized by matrix isolation FTIR spectroscopy. On photolysis, the Fe atoms could further insert into the OH bonds in H_2O molecules with a stepwise pattern to form multi metal−oxo core species including HFeOFeH, HFeOFeOH, and possibly HFeOFeOFeH, which were identified by isotopic substitutions and density functional calculations. Reactions of FeO with H_2 also lead to HFeOH as the primary product. In addition, a potential energy surface for the Fe + H_2O ⇔ FeO + H_2 reaction was constructed to elucidate the reaction mechanisms.

Introduction

During the past decade, extensive experimental and theoretical studies have been carried out concerning the reactivity of MO^+ with H_2 and M^+ with H_2O (M denotes transition metals).[1−11] By contrast, the reactions of neutral metal atoms with H_2O and metal oxides with H_2 have received far less attention. Lin and Parson reported that atomic Sc reacted with water to give ScO in gas phase.[12] Using the matrix isolation infrared absorption method, Kauffman et al. showed that thermal Sc, Ti, and V atoms could react with water to form insertion products spontaneously, while metal monoxides were formed on photolysis. The later transition metal atoms formed adducts with water, which rearranged to insertion molecules on photolysis.[13] A recent gas-phase kinetic study showed that ground-state FeO did not react with H_2.[14] On the theoretical side, Siegbahn et al. have studied the reactivity trends of the second row transition metals with H_2O.[15] Bonding of water to copper and nickel atoms has also been studied by density functional calculations.[16] More recently, we have performed matrix isolation FTIR and theoretical studies on the reactions of Sc,[17] Ti,[18a] and V[18b] group and Mn[19] metal atoms with H_2O, different reaction paths leading to H_2MO and MO + H_2 and several important reaction intermediates were observed. Compared with previous gas phase reactions of metal cations, our studies showed that the chemistry of neutral metal atoms is distinctly different from that of metal ions. In particular, the combination of matrix-isolation FTIR spectroscopy and quantum chemical calculations is very powerful in elucidating the reaction mechanism. In this paper, the reactions of Fe atoms with H_2O and FeO with H_2 are studied in detail. Various reaction intermediates and products are identified and a detailed potential energy surface for the Fe + H_2O ⇔ FeO + H_2 reaction is constructed using density functional theoretical (DFT) calculations. The results have been compared with our earlier works covering the Sc, Ti, V, and Mn + H_2O reactions to observe existent trends for transition metal−water reactions.

* Corresponding author. FAX: +86-21-65102777. E-mail: mfzhou@fudan.edu.cn.

Experimental and Theoretical Methods

The experimental setup for pulsed laser ablation and matrix infrared spectroscopic investigation has been described previously.[17,18] Briefly, a 1064 nm Nd:YAG laser fundamental (Spectra Physics, DCR 150, 20 Hz repetition rate and 8 ns pulse width) was focused onto the rotating Fe or Fe_2O_3 target through a hole in a CsI window. The ablated species were co-deposited with H_2O or H_2 in excess argon onto a 11 K CsI window, which was mounted on a cold tip of a closed-cycle helium refrigerator (Air Products, Model CSW202) for 1 h at a rate of approximately 4−5 mmol/h. Typically, the laser beam was focused onto a spot of about 0.25 mm^2 on the target with 5−10 mJ/pulse laser power. H_2O, $H_2{}^{18}O$ (96% ^{18}O), and D_2O were subjected to several freeze−pump−thaw cycles before use. Infrared spectra were recorded on a Bruker IFS113v spectrometer at 0.5 cm^{-1} resolution using a DTGS detector. Matrix samples were annealed at different temperatures, and selected samples were subjected to broad-band photolysis using a 250 W high pressure Hg lamp.

Quantum chemical calculations were performed using the Gaussian 98 program.[20] The three-parameter hybrid functional according to Becke with additional correlation corrections due to Lee, Yang, and Parr were utilized (B3LYP).[21,22] The 6-311++G(d,p) basis sets were used for H and O atoms, and the all-electron basis sets of Wachter−Hay as modified by Gaussian were used for Fe atom.[23,24] Reactants, various intermediates, and products were optimized without structural constraints. Harmonic vibrational frequencies and intensities were calculated with analytic second derivatives, and zero point vibrational energies (ZPVE) were derived. Transition state optimizations were performed using the synchronous transit-guided quasi-Newton (STQN) method.[25] The algorithm can generate a guess for the transition structure that is midway between the reactant and product, and it then goes on to optimize that starting structure to a first-order saddle point. Energies are all corrected with ZPVE.

10.1021/jp010914n CCC: $20.00
Published on Web 06/29/2001

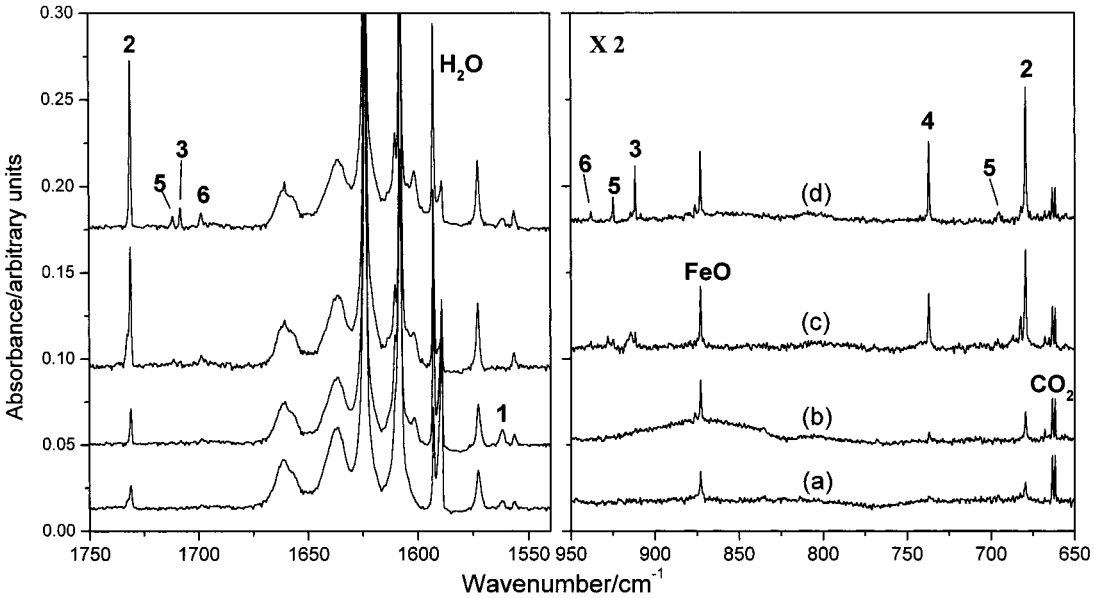

Figure 1. Infrared spectra in the 1750−1540 and 950−650 cm^{-1} regions from co-deposition of laser-ablated Fe with H_2O in excess Ar: (a) 1 h sample deposition; (b) 25 K annealing; (c) 20 min Hg lamp photolysis; (d) 30 K annealing.

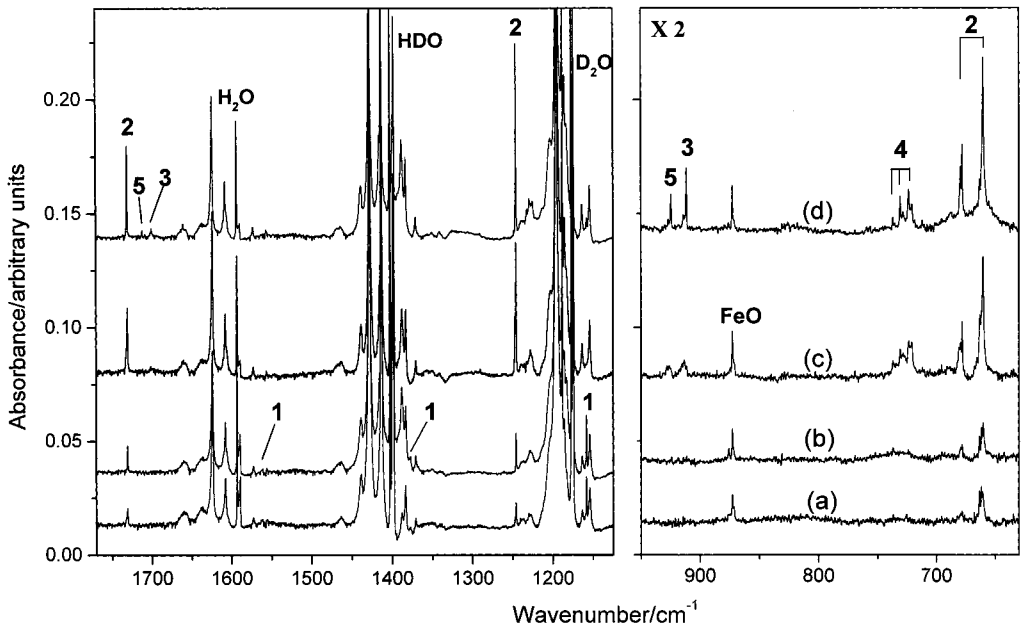

Figure 2. Infrared spectra in the 1775−1125 and 950−630 cm^{-1} regions from co-deposition of laser-ablated Fe with H_2O/HDO/D_2O in excess Ar: (a) 1 h sample deposition; (b) 25 K annealing; (c) 20 min Hg lamp photolysis; (d) 30 K annealing.

Results and Discussion

Infrared Spectra. *Fe + H_2O/Ar.* Representative spectra from co-condensation of laser-ablated Fe atoms with H_2O in excess argon are shown in Figure 1, and the band positions are summarized in Table 1. After sample deposition, new product absorptions at 1731.0, 1561.9, and 679.7 cm^{-1} (labeled as **1** and **2**) together with FeO absorptions at 872.8 cm^{-1} were observed.[26] Broad-band photolysis destroyed the 1561.9 cm^{-1} band, markedly increased the 1731.0, 679.7, and FeO absorptions, and produced new absorptions at 1708.0, 911.8, 1711.6, 925.0, 1698.6, 938.1, and 737.3 cm^{-1} as labeled **3**−**6** in Figure 1. Isotopic substitution was employed for band identification, and the results are also listed in Table 1. Figures 2 and 3 show the mixed H_2O + HDO + D_2O and $H_2{}^{16}O$ + $H_2{}^{18}O$ spectra in selected regions.

FeO + H_2/Ar. Experiments were done with an Fe_2O_3 target and pure argon. The major product absorptions observed after sample deposition was a 872.8 cm^{-1} band due to FeO; minor FeO_2 (945.7 cm^{-1}) and FeOFe (868.6 cm^{-1}) absorptions were observed as well.[26,27] Similar experiments were performed with laser ablation of Fe_2O_3 in 1.0% H_2 in argon, and the spectra in

TABLE 1: Observed Product Band Positions (cm^{-1}) from Co-deposition of Laser-ablated Fe Atoms with H_2O/Ar

H_2O	D_2O	$H_2{}^{18}O$	assignment
1561.9	1158.2	1555.0	(**1**) $FeOH_2$
1731.0	1245.9	1731.0	(**2**) HFeOH
679.7	660.4	654.2	(**2**) HFeOH
1708.0	1229.2	1708.0	(**3**) HFeOFeH
911.8	911.8	866.8	(**3**) HFeOFeH
737.3	723.9	714.5	(**4**) $Fe(OH)_2$
1711.6	1232.3	1711.6	(**5**) HFeOFeOH
925.0	925.0	880.0	(**5**) HFeOFeOH
695.5		667.9	(**5**) HFeOFeOH
1698.6			(**6**) HFeOFeOFeH
938.1			(**6**) HFeOFeOFeH

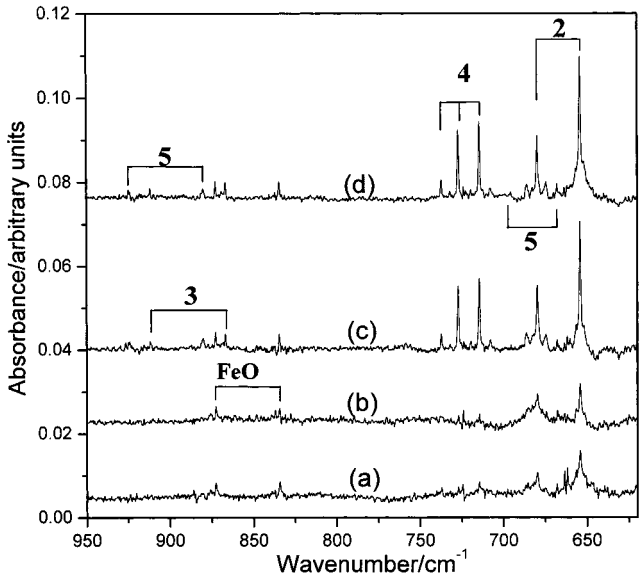

Figure 3. Infrared spectra in the 950−620 cm^{-1} regions from co-deposition of laser-ablated Fe with $H_2O/H_2{}^{18}O$ in excess Ar: (a) 1 h sample deposition; (b) 25 K annealing; (c) 20 min Hg lamp photolysis; (d) 30 K annealing.

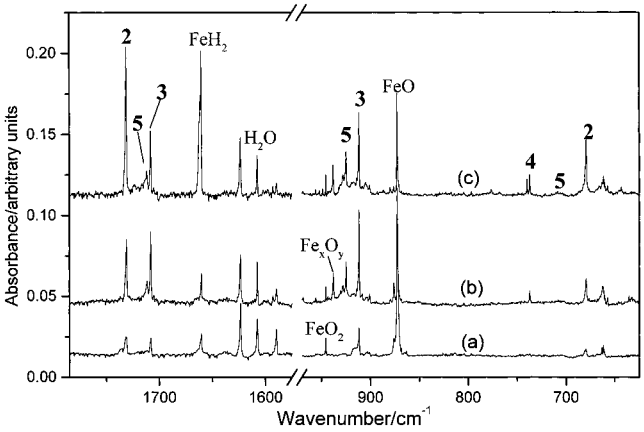

Figure 4. Infrared spectra in the 1780−1570 and 970−630 cm^{-1} regions from co-deposition of laser-ablated FeO with H_2 in excess Ar: (a) 1 h sample deposition; (b) 25 K annealing; (c) 20 min Hg lamp photolysis.

selected regions are shown in Figure 4. Besides the metal oxide absorptions, new product absorptions were observed (as labeled **2**−**5** in Figure 4). These new absorptions increased on annealing and photolysis. Photolysis also produced FeH_2 absorptions at 1660.5 cm^{-1}.[28]

Calculation Results. B3LYP/6-311++G(d,p) calculations were done for three FeH_2O isomers, namely, the $FeOH_2$ and (η^2-H_2)FeO complexes and the inserted HFeOH molecule, on both quintet and triplet states. All three FeH_2O isomers were predicted to have quintet ground states. The $^5A'$ HFeOH is the most stable isomer, followed by the $^5A'$ $FeOH_2$ and $^5A_2$ (η^2-H_2)FeO, which were predicted to be 27.6 and 44.6 kcal/mol higher in energy than the $^5A'$ HFeOH. The optimized geometric parameters are shown in Figure 5, and the vibrational frequencies and intensities are given in Table 2. Similar calculations were also done on $Fe(OH)_2$, HFeOFeH, HFeOFeOH, and HFeOFeOFeH molecules. The optimized geometries are also shown in Figure 5, and the vibrational frequencies and intensities are listed in Table 3.

Product Assignments. *$FeOH_2$.* The weak 1561.9 cm^{-1} band in the Fe + H_2O/Ar experiments is assigned to the H_2O bending

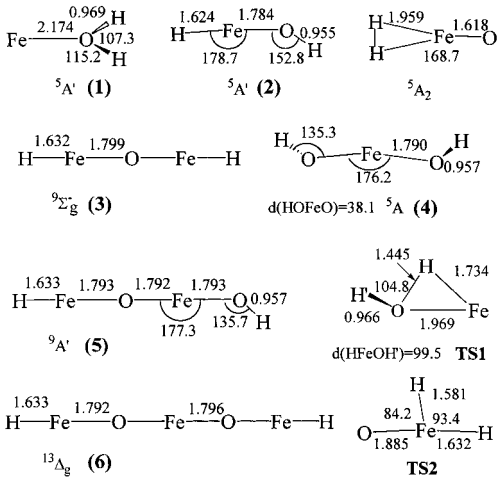

Figure 5. B3LYP/6-311++G(d,p) optimized geometric parameters (bond length in angstroms, bond angle in degrees) of the reaction products.

TABLE 2: Calculated Vibrational Frequencies (cm^{-1}) and IR Intensities (km/mol, in Parentheses) for the Reaction Intermediates and Transition States of the Fe + H_2O → FeO + H_2 Reaction System

$FeOH_2$ ($^5A'$)	HFeOH ($^5A'$)	(H_2)FeO ($^5A_2$)	TS1	TS2
3802 (64, a″)	3972 (145, a′)	4038 (18, a_1)	1195i (1352)	118.4i (121)
3691 (98, a′)	1801 (248, a′)	987 (26, b_2)	407.3 (154)	141.0 (22)
1592 (83, a′)	708 (128, a′)	922 (147, a_1)	513.4 (147)	331.0 (41)
399 (6, a″)	287 (200, a′)	592 (16, a_1)	752.0 (71)	906.3 (64)
290 (215, a′)	286 (214, a′)	168 (0, b_2)	1525.7 (12)	1816.4 (72)
248 (1, a′)	200 (83, a′)	51 (0, b_1)	3785.0 (47)	1889.0 (19)

vibration of the $FeOH_2$ complex, in agreement with previous assignment.[13] This band, observed after sample deposition, increased readily on sample annealing and disappeared upon broad-band photolysis. It shifted to 1158.0 cm^{-1} with D_2O and to 1555.0 cm^{-1} with $H_2{}^{18}O$. The isotopic H/D ratio of 1.3641 and $^{16}O/^{18}O$ ratio of 1.0044 also indicate a H_2O bending vibration. Density functional calculations predicted this molecule to have a $^5A'$ electronic ground state with a nonplanar structure, as shown in Figure 5. The H_2O bending vibrational frequency was calculated to be 1592 cm^{-1}, which requires a scaling factor (observed frequency divided by calculated frequency) of 0.981 to fit the observed value. As listed in Table 4, the calculated isotopic frequency ratios are also in good agreement with the experimental values. The $^5A'$ ground-state $FeOH_2$ is derived from a mixture of the ^5D iron ground state and ^5F state, as can be seen from the 3d population of 6.40 electrons. The ^5F state is about 20.2 kcal/mol higher in energy than the ^5D ground state.[29] The promotion of the 4s electron to the 3d orbital reduces the Fe−OH_2 repulsion at a cost of additional promotion energy.

HFeOH. Sharp bands at 1731.0 and 679.7 cm^{-1} are assigned to the Fe−H and Fe−OH stretching vibrations of the HFeOH molecule, which are in agreement with the previous report.[13] These two bands appeared in both the Fe + H_2O and FeO + H_2 reactions, and increased greatly in concert upon UV photolysis. The upper mode underwent a large (485.1 cm^{-1}) deuterium shift and a negligible oxygen-18 shift, indicating that this vibration is due to Fe−H stretching. The lower mode shifted to 660.4 cm^{-1} with D_2O and to 654.2 cm^{-1} with $H_2{}^{18}O$, and gave an isotopic H/D ratio of 1.0292 and an $^{16}O/^{18}O$ ratio of 1.0390, which are characteristic of an Fe−OH stretching mode.

Recent study by Rollason and Plane[14] predicted the HFeOH molecule to have a $^5\Sigma$ ground state with linear structure at the B3LYP/6-311G level. However, our DFT calculations at the same level of theory found the ground state to be $^5\Delta$ with the

TABLE 3: Calculated Vibrational Frequencies (cm^{-1}) and IR Intensities (km/mol) of the $Fe(OH)_2$, HFeOFeH, HFeOFeOH, and HFeOFeOFeH Molecules

species	vibrational frequency (intensity, mode)
$Fe(OH)_2$ (^5A)	3939 (22, a), 3938 (20, b), 761 (240, b), 631 (2, a), 439 (83, a), 407 (258, b), 146 (9, b), 144 (8, a), 99 (95, a)
HFeOFeH ($^9\Sigma_g^-$)	1788 (0, σ_g), 1775 (674, σ_u), 882 (882, σ_u), 343 (0, σ_g), 256 (0, π_g), 249 (622, π_u), 90 (0, π_g)
HFeOFeOH ($^9A'$)	3941 (126, a′), 1777 (323, a′), 898 (921, a′), 702 (118, a′), 415 (182, a′), 321 (5, a′), 249 (177, a″), 246 (166, a′), 161 (7, a″), 156 (10, a′), 74 (2, a″), 68 (1, a′)
HFeOFeOFeH ($^{13}\Delta_g$)	1779 (0, σ_g), 1776 (700, σ_u), 907 (0, σ_g), 880 (2146, σ_u), 419 (1, σ_u), 249 (666, π_u), 247 (0, π_g), 237 (0, σ_g), 164 (18, π_u), 89 (0, π_g), 32 (0, π_u)

TABLE 4: Scaling Factors and Observed and Calculated Isotopic Vibrational Frequency Ratios of the Major Reaction Products

			H/D		$^{16}O/^{18}O$	
molecule	mode	scaling factor	obsd	calcd	obsd	calcd
(**1**) $FeOH_2$	OH_2 bend.	0.981	1.3486	1.3641	1.0044	1.0043
(**2**) HFeOH	Fe−H	0.961	1.3894	1.4018	1.0000	1.0000
	Fe−OH	0.960	1.0292	1.0267	1.0390	1.0423
(**3**) HFeOFeH	Fe−H	0.962	1.3895	1.4027	1.0000	1.0001
	FeOFe	1.034	1.0000	1.0000	1.0519	1.0526
(**4**) $Fe(OH)_2$	Fe−OH	0.969	1.0185	1.0196	1.0319	1.0328
(**5**) HFeOFeOH	Fe−H	0.963	1.3889	1.4021	1.0000	1.0001
	FeOFe	1.029	1.0000	1.0002	1.0511	1.0516
	Fe−OH	0.990		1.0229	1.0413	1.0398

valence configuration of $(3d\delta)^3(3d\pi)^2(3d\sigma + 4s)^1$. The $^5\Sigma^+$ state with the configuration of $(3d\delta)^2(3d\pi)^2(3d\sigma + 4s)^2$ was predicted to be 3.6 kcal/mol higher in energy than the $^5\Delta$ state. At the B3LYP/6-311++G(d,p) level of theory, the $^5\Sigma^+$ state was predicted to be 11.2 kcal/mol higher in energy than the $^5\Delta$ state. At this level of theory, both states are proved to be saddle points on the potential energy surface with one imaginary bending frequency. Along with this bending mode, a $^5A'$ state with bent geometry was predicted to be the local minimum and is about 0.1 kcal/mol lower in energy than the linear $^5\Delta$ state. As listed in Table 2, the Fe−H and Fe−OH stretching vibrational frequencies for $^5A'$ state HFeOH were calculated to be 1801 and 708 cm^{-1}, which require scaling factors of 0.961 and 0.960 to fit the experimental values. The calculated isotopic ratios (upper mode: H/D = 1.4018, $^{16}O/^{18}O$ = 1.0000; lower mode: H/D = 1.0267, $^{16}O/^{18}O$ = 1.0423) are in good agreement with the observed values.

HFeOFeH. The 1708.0 and 911.8 cm^{-1} bands are assigned to the antisymmetric Fe−H and Fe−O−Fe stretching vibrations of the HFeOFeH molecule, based on previous assignment[13] and present experimental and theoretical results. These two bands were produced together upon Hg arc irradiation in Fe + H_2O/Ar experiments, but in FeO + H_2/Ar experiments this set of bands appeared after sample deposition and increased on annealing. The isotopic experiments showed that the upper mode is due to an Fe−H stretching vibration. The lower mode exhibited large oxygen-18 isotopic shift, and the $^{16}O/^{18}O$ ratio of 1.0519 is larger than that of diatomic FeO ratio (1.0462). The isotopic data also indicate that only one oxygen atom is involved. The oxygen isotopic ratio is similar to that of the FeOFe species[27] and implies that this band is due to an antisymmetric Fe−O−Fe stretching vibration.

The assignment is strongly supported by DFT calculations. As depicted in Figure 5, the HFeOFeH molecule was calculated to have a $^9\Sigma_g^-$ ground state with linear structure. The antisymmetric Fe−H and Fe−O−Fe stretching vibrations were predicted at 1775 and 882 cm^{-1} with the calculated isotopic ratios (upper mode H/D = 1.4027, lower mode $^{16}O/^{18}O$ = 1.0526) in excellent agreement with the observed values.

$Fe(OH)_2$. The 737.3 cm^{-1} band appeared on photolysis in Fe + H_2O/Ar experiments; it shifted to 723.9 cm^{-1} with D_2O and to 714.5 cm^{-1} with $H_2{}^{18}O$. The isotopic ratios H/D = 1.0185 and $^{16}O/^{18}O$ = 1.0319 suggest an Fe−OH stretching vibration. In experiments using H_2O/HDO/D_2O and $H_2O/H_2{}^{18}O$ mixed reagents, triplet features were produced, suggesting that two equivalent OH subunits are involved. This band is assigned to the antisymmetric Fe−OH stretching vibration of the $Fe(OH)_2$ molecule. In agreement with a recent report,[30] the $Fe(OH)_2$ molecule was predicted to have a ^5A electronic ground state with C_2 symmetry. The antisymmetric Fe−OH stretching vibration was calculated at 761.3 cm^{-1}, which requires a scaling factor of 0.969 to fit the measured band position.

HFeOFeOH. Weak bands at 1711.6, 925.0, and 695.5 cm^{-1} appeared only on broad-band photolysis in the Fe + H_2O/Ar experiments. The 1711.6 cm^{-1} band shifted to 1232.3 cm^{-1} with D_2O, and the H/D ratio of 1.3889 indicates an Fe−H stretching vibration. The 925.0 cm^{-1} band showed no deuterium shift, but shifted to 880.0 cm^{-1} with $H_2{}^{18}O$ and gave an $^{16}O/^{18}O$ ratio of 1.0511, which suggests an antisymmetric Fe−O−Fe stretching vibration analogous to the HFeOFeH. The 695.5 cm^{-1} band is due to an Fe−OH stretching vibration, and only one OH subunit is involved as judged by the doublet structure in the mixed H_2O + $H_2{}^{18}O$ spectrum. These three bands are assigned to the HFeOFeOH molecule. As shown in Figure 5, the HFeOFeOH molecule was calculated to have a $^9A'$ ground state with Fe−H, Fe−O−Fe, and Fe−OH stretching vibrations at 1777, 898, and 702 cm^{-1}, which are in good accord with the observed band positions. As for HFeOFeH molecule, the antisymmetric Fe−O−Fe stretching vibration is slightly underestimated.

(HFeOFeOFeH). Weak bands at 1698.6 and 938.1 cm^{-1} produced on photolysis in the Fe + H_2O system are tentatively assigned to the Fe−H and O−Fe−O stretching vibrations of the HFeOFeOFeH molecule. The isotopic counterparts of these bands are too weak to be observed, and make a definite assignment impossible. Our DFT calculations on this molecule found a stable $^{13}\Delta_g$ ground state with linear geometry. The most intense vibrations were predicted to be the Fe−H and OFeO stretching vibrations, with frequencies at 1776 and 880 cm^{-1}, respectively.

The bonding characters of above multimetal core species HFeOFeH, HFeOFeOH, and HFeOFeOFeH are quite similar. As the ground state of Fe atom has $3d^64s^2$ valence electron configuration, in order to satisfy the valence of H and O, the two 4s electrons of Fe are used to form covalent bonds with H

TABLE 5: Calculated Atomic Spin Density and Mulliken Population of 3d Orbitals on the Fe Centers

	spin density		3d population	
	Fe^1	Fe^2	Fe^1	Fe^2
HFeOFeH	4.00		6.24	
HFe^1OFe^2OH	3.99	3.83	6.24	6.29
HFe^1OFe^2OFeH	3.99	3.91	6.25	6.28

and O atoms, and the Fe 3d electrons remain unpaired. Consistent with this simple valence bonding model, our DFT calculations predicted that these molecules have high spin ground states: $S = 8/2$ for HFeOFeH and HFeOFeOH, and $S = 12/2$ for HFeOFeOFeH. As listed in Table 5, the unpaired electrons are essentially located on the Fe centers. The Mulliken population analysis showed that the iron centers exhibited electronic configurations very close to d^6. This bonding feature is very similar to the analogous HMnOMnH, HMnOMnOH, and HMnOMnOMnH molecules identified recently.[18] It is interesting to note that, for Mn and Fe, the energy separation between states with configurations $3d^{n-2}4s^2$ and $3d^{n-1}4s^1$ is quite large: 49.5 kcal/mol for Mn and 20.2 kcal/mol for Fe,[29] which makes the 4s−3d hybridization inefficient. Similar multimetal core species were not observed in other transition metal−water reaction systems.[13,17,18]

Reaction Mechanism. Scheme 1 summarizes the genetic reaction paths involving the observed products. Thermodynamic properties of the above-mentioned reactions were evaluated by DFT calculations. Apparently, formation of these species is favored from the energy point of view:

$$Fe(^5D) + H_2O \rightarrow FeOH_2(^5A') \Delta E = -13.5 \text{ kJ/mol} \quad (1)$$

$$FeOH_2(^5A') \rightarrow HFeOH(^5A') \Delta E = -27.6 \text{ kJ/mol} \quad (2)$$

$$FeO(^5\Delta) + H_2 \rightarrow HFeOH(^5A') \Delta E = -48.6 \text{ kJ/mol} \quad (3)$$

$$Fe(^5D) + HFeOH(^5A') \rightarrow HFeOFeH(^9\Sigma_g^-) \quad \Delta E = -45.9 \text{ kJ/mol} \quad (4)$$

$$Fe(^5D) + 2H_2O \rightarrow Fe(OH)_2(^5A) + H_2 \Delta E = -62.7 \text{ kJ/mol} \quad (5)$$

$$Fe(^5D) + Fe(OH)_2(^5A) \rightarrow HFeOFeOH(^9A') \quad \Delta E = -46.4 \text{ kJ/mol} \quad (6)$$

$$Fe(^5D) + HFeOFeOH(^9A') \rightarrow HFeOFeOFeH(^{13}\Delta_g) \quad \Delta E = -46.2 \text{ kJ/mol} \quad (7)$$

In Fe + H_2O experiments, the yield of $FeOH_2$ complex increased on annealing, suggesting that ground state ^6D Fe atoms react with water to form the $FeOH_2$ complex spontaneously, via reaction 1, which was predicted to be exothermic by about 13.5 kcal/mol. The increase of HFeOH absorptions upon photobleaching of $FeOH_2$ implies that HFeOH is generated from $FeOH_2$, via reaction 2. The HFeOFeH absorptions appeared on photolysis, suggesting that Fe atoms can further insert into the O−H bond of HFeOH via reaction 4, which was predicted to be exothermic by about 45.9 kcal/mol. The $Fe(OH)_2$ molecules are most probably formed in reaction 5 of Fe atoms with water dimer $(H_2O)_2$. This reaction was calculated to be exothermic by about 62.7 kcal/mol. Upon photolysis, Fe atoms can further insert into the O−H bonds of $Fe(OH)_2$ to form the HFeOFeOH and HFeOFeOFeH molecules, in reactions 6 and 7, which were also predicted to be highly exothermic.

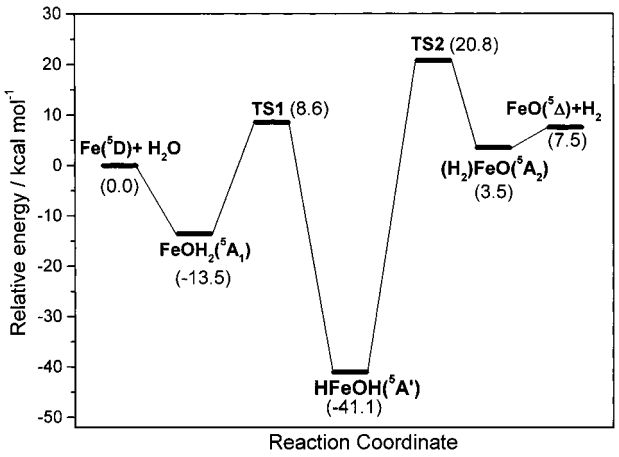

Figure 6. Potential energy surface following the Fe + $H_2O \rightarrow$ FeO + H_2 reaction path. Energies are in kilocalories per mole and are relative to the separated ground-state reactants: Fe(^{6}D) + $H_2O(^1A_1)$. Energies are corrected with zero point vibrational energies (ZPVE).

SCHEME 1

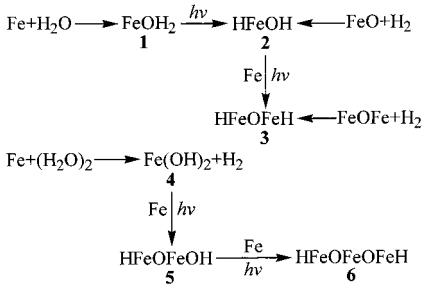

In FeO + H_2/Ar experiments, laser ablation of Fe_2O_3 target produced FeO as the major product, with minor FeO_2 and FeOFe. The HFeOH molecules are mainly formed via reaction 3 between FeO and H_2. The HFeOH absorptions increased on annealing, suggesting that reaction 3 proceeds spontaneously. The HFeOFeH molecules are mostly formed by reactions between FeOFe and H_2.

The potential energy surface (PES) following the Fe + $H_2O \rightarrow$ FeO + H_2 reaction path has been calculated at the B3LYP/6-311++G(d,p) level of theory, as shown in Figure 6. The first step of Fe and H_2O interaction is the formation of the $FeOH_2$ complex. Starting from the $FeOH_2$ complex, one hydrogen atom transfers from the oxygen to the Fe center, leading to the HFeOH intermediate through transition state 1 (TS1). This transition state was predicted to lie 8.6 kcal/mol higher in energy than the ground-state reactants Fe + H_2O. The HFeOH could further rearrange to form the (η^2-H_2)FeO complex through transition state 2 (TS2). From (η^2-H_2)FeO, the loss of H_2 proceeds without transition state to FeO + H_2. The TS2 lies 20.8 kcal/mol higher in energy than the Fe + H_2O reactants. The optimized structures for these transition states are shown in Figure 5, and the calculated vibrational frequencies are summarized in Table 2.

The reaction from HFeOH to FeO + H_2 was predicted to be endothermic by about 48.6 kcal/mol, and there is an about 62.0 kcal/mol energy barrier. By contrast, the reverse reaction is exothermic and has only about 13.3 kcal/mol energy barrier. In Fe + H_2O experiments, the FeO absorption was increased only on broad-band photolysis. In FeO + H_2/Ar experiments, the HFeOH absorptions increased on annealing, which also suggests a low reaction energy barrier for reaction 3. Although the (η^2-H_2)FeO complex was predicted to be stable, it was not observed in our experiments. This (η^2-H_2)FeO complex was predicted by DFT calculation to have a $^5A_2$ ground state with

C_{2v} symmetry. The binding energy with respect to FeO + H_2 was calculated to be only 4.0 kcal/mol.

The reaction features for iron are very similar to those of Mn,[18] but are quite different from those of early transition metals Sc, Ti, and V with H_2O as reported previously by our group.[17,18] For Sc, Ti, and V atoms, the insertion molecules HMOH (M = Sc, Ti, and V) were produced spontaneously, and the MOH_2 complexes were not observed. These complexes are metastable species; they will rapidly rearrange to the HMOH molecules as soon as they are formed, as the HMOH formation reactions are highly exothermic with low reaction energy barriers. For both Mn and Fe, the $MnOH_2$ and $FeOH_2$ complexes are stable intermediates, as the reactions from $MnOH_2$ and $FeOH_2$ to HMnOH and HFeOH have quite high energy barrier.

From HMOH, the formation of ScO + H_2 is the only reaction channel for Sc, and two reaction paths coexist for Ti and V systems: the formation of covalently bonded H_2TiO or H_2VO and the production of TiO + H_2 or VO + H_2. The potential energy surfaces for the Ti + H_2O and V + H_2O reactions involve spin−orbit coupling, which is responsible for the formation of lower spin state H_2TiO and H_2VO molecules. The H_2TiO and H_2VO channel is energetically favored over the TiO and VO channel, as Ti and V group elements tend to form higher oxidation states. For Mn and Fe systems, the Mn + H_2O and Fe + H_2O reactions take place only on high spin states. The formation of monoxide is either slightly endothermic or exothermic, and is the only reaction channel observed. The formation of covalently bonded H_2MnO or H_2FeO requires spin crossing and is energetically unfavorable due to the stability of the d^5 and d^6 electronic configurations of Mn and Fe atoms. In contrast, both Mn and Fe atoms prefer to insert into the O−H bonds to form dimetal− or trimetal−oxo core species. Apparently, the 3d electrons of early transition metals are inclined to participate in reaction, while only the 4s electrons are involved in the cases of Mn and Fe.

Conclusions

The reactions of Fe atoms with H_2O and FeO with H_2 have been studied using matrix isolation FTIR and density functional theoretical calculations. In agreement with previous thermal atom experiments, laser-ablated Fe atoms reacted with H_2O to form the $FeOH_2$ and HFeOH molecules as characterized by matrix isolation FTIR spectroscopy. On photolysis, the Fe atoms could further insert into the OH bonds in H_2O molecules with a stepwise pattern to form multi metal−oxo core species including HFeOFeH, HFeOFeOH, and possibly HFeOFeOFeH. Reactions of FeO with H_2 also lead to HFeOH as the primary product. Characterization of these di and trimetal species may shed some light on the nature of the reactions of iron−oxo core for H_2O oxidation. Furthermore, an in-depth analysis of the potential energy surface following the Fe + $H_2O \rightarrow$ FeO + H_2 reaction path was given, including various minima and several important transition states. The results have been compared with our earlier works covering the Sc, Ti, V, and Mn + H_2O reactions, and several existent trends are drawn:

(1) For reactions between earlier transition metals and water molecules, two exothermic reaction paths leading to the covalently bonded H_2MO and the MO + H_2 (M = Ti, V) were observed. The potential energy surfaces involve spin−orbit coupling, which is responsible for the formation of lower spin state H_2MO molecules. For Fe and Mn, reactions take place only on high spin states, and the formation of monoxide is the only reaction channel observed;

(2) Due to different valence electron configurations, the 3d electrons of early transition metals are inclined to participate in reaction to form higher oxidation states; thus the H_2MO channel is energetically favored over the MO + H_2 channel. In contrast, both Mn and Fe atoms prefer to insert into the O−H bonds to form dimetal− or trimetal−oxo core species, and only the 4s electrons are involved in bonding.

Acknowledgment. This work is supported by NSFC (Grant No. 20003003) and the Chinese NKBRSF.

References and Notes

(1) Schroder, D.; Shaik, S.; Schwarz, H. *Acc. Chem. Res.* **2000**, *33*, 139.

(2) (a) Irigoras, A.; Fowler, J. E.; Ugalde, J. M. *J. Am. Chem. Soc.* **1999**, *121*, 574; (b) *J. Am. Chem. Soc.* **1999**, *121*, 8549; (c) *J. Am. Chem. Soc.* **2000**, *122*, 114; (d) *J. Phys. Chem. A* **1998**, *102*, 293.

(3) (a) Danovich, D.; Shaik, S. *J. Am. Chem. Soc.* **1997**, *119*, 1773. (b) Filatov, M.; Shaik, S. *J. Phys. Chem. A* **1998**, *102*, 3835.

(4) Schroder, D.; Fiedler, A.; Ryan, M. F.; Schwarz, H. *J. Phys. Chem.* **1994**, *98*, 68.

(5) Clemmer, D. E.; Chen, Y. M.; Armentrout, P. B. *J. Phys. Chem.* **1994**, *98*, 6522. Chen, Y. M.; Clemmer, D. E.; Armentrout, P. B. *J. Phys. Chem.* **1994**, *98*, 11490.

(6) (a) Schroder, D.; Schwarz, H. *Angew. Chem., Int. Ed. Engl.* **1995**, *34*, 1973. (b) Ryan, M. F.; Fielder, A.; Schroder, D.; Schwarz, H. *J. Am. Chem. Soc*. **1995**, *117*, 2033.

(7) Kang, H.; Beauchamp, J. L. *J. Am. Chem. Soc.* **1986**, *108*, 5663.

(8) Clemmer, D. E.; Aristov, N.; Armentrout, P. B. *J. Phys. Chem.* **1993**, *97*, 544.

(9) Tilson, J. L.; Harrison, J. F. *J. Phys. Chem.* **1991**, *95*, 5097.

(10) (a) Rosi, M.; Bauschlicher, C. W., Jr. *J. Chem. Phys*. **1989**, *90*, 7264. (b) *J. Chem. Phys*. **1990**, *92*, 1876.

(11) Ye, S. *J. Mol. Struct. (THEOCHEM)* **1997**, *417*, 157.

(12) Liu, K.; Parson, J. M. *J. Chem. Phys.* **1978**, *68*, 1794.

(13) (a) Kauffman, J. W.; Hauge, R. H.; Margrave, J. L. *J. Phys. Chem.* **1985**, *89*, 3541; (b) *J. Phys. Chem.* **1985**, *89*, 3547.

(14) Rollason, R. J.; Plane, J. M. C. *Phys. Chem. Chem. Phys.* **2000**, *2*, 2335

(15) Siegbahn, P. E. M.; Blomberg, M. R. A.; Svensson, M. *J. Phys. Chem.* **1993**, *97*, 2564.

(16) Adamo, C.; Lelj, F. *J. Mol. Struct. (THEOCHEM)* **1997**, *389*, 83.

(17) Zhang, L. N.; Dong, J.; Zhou, M. F. *J. Phys. Chem. A* **2000**, *104*, 8882;

(18) (a) Zhou, M. F.; Zhang, L. N.; Dong, J.; Qin, Q. Z. *J. Am. Chem. Soc.* **2000**, *122*, 10680; (b) *J. Am. Chem. Soc.* **2001**, *123*, 135.

(19) Zhou, M. F.; Zhang, L. N.; Shao, L. M.; Wang, W. N.; Fan, K. N.; Qin, Q. Z. *J. Phys. Chem. A*, in press.

(20) Frisch, M. J.; Trucks, G. W.; Schlegel, H. B.; Scuseria, G. E.; Robb, M. A.; Cheeseman, J. R.; Zakrzewski, V. G.; Montgomery, Jr., J. A.; Stratmann, R. E.; Burant, J. C.; Dapprich, S.; Millam, J. M.; Daniels, A. D.; Kudin, K. N.; Strain, M. C.; Farkas, O.; Tomasi, J.; Barone, V.; Cossi, M.; Cammi, R.; Mennucci, B.; Pomelli, C.; Adamo, C.; Clifford, S.; Ochterski, J.; Petersson, G. A.; Ayala, P. Y.; Cui, Q.; Morokuma, K.; Malick, D. K.; Rabuck, A. D.; Raghavachari, K.; Foresman, J. B.; Cioslowski, J.; Ortiz, J. V.; Baboul, A. G.; Stefanov, B. B.; Liu, G.; Liashenko, A.; Piskorz, P.; Komaromi, I.; Gomperts, R.; Martin, R. L.; Fox, D. J.; Keith, T.; Al-Laham, M. A.; Peng, C. Y.; Nanayakkara, A.; Gonzalez, C.; Challacombe, M.; Gill, P. M. W.; Johnson, B.; Chen, W.; Wong, M. W.; Andres, J. L.; Gonzalez, C.; Head-Gordon, M.; Replogle, E. S.; Pople, J. A. *Gaussian 98*, Revision A.7; Gaussian, Inc.: Pittsburgh, PA, 1998.

(21) Becke, A. D. *J. Chem. Phys*. **1993**, *98*, 5648.

(22) Lee, C.; Yang, E.; Parr, R. G. *Phys. Rev. B* **1988**, *37*, 785.

(23) McLean, A. D.; Chandler, G. S. *J. Chem. Phys.* **1980**, *72*, 5639. Krishnan, R.; Binkley, J. S.; Seeger, R.; Pople, J. A. *J. Chem. Phys*. **1980**, *72*, 650.

(24) Wachter, J. H. *J. Chem. Phys.* **1970**, *52*, 1033. Hay, P. J. *J. Chem. Phys*. **1977**, *66*, 4377.

(25) (a) Peng, C.; Ayala, P. Y.; Schlegel, H. B.; Frisch, M. J. *J. Comput. Chem.* **1996**, *17*, 49. (b) Peng, C.; Schlegel, H. B. *Isr. J. Chem.* **1994**, *33*, 449.

(26) See, for example: Green, D. W.; Reedy, G.T. *J. Mol. Spectrosc.* **1979**, *78*, 257.

(27) Chertihin, G. V.; Saffel, W.; Yustein, J. T.; Andrews, L.; Neurock, M.; Ricca, A.; Bauschlicher, C. W., Jr. *J. Phys. Chem.* **1996**, *100*, 5261 and references therein.

(28) Chertihin, G. V.; Andrews, L. *J. Phys. Chem.* **1995**, *99*, 12131 and references therein.

(29) Sugar, J.; Musgrove, A. *J. Phys. Chem. Ref. Data* **1990**, *19*, 527.

(30) Kellogg, C. B.; Irikura, K. K. *J. Phys. Chem. A* **1999**, *103*, 1150.